J. Fluid Mech. (2014), *vol.* 757, *pp.* 432–457.
doi:10.1017/jfm.2014.496

Influence of Stokes number on the velocity and concentration distributions in particle-laden jets

Timothy C. W. Lau[1,†] **and Graham J. Nathan**[1]

[1]Centre for Energy Technology, School of Mechanical Engineering, The University of Adelaide, SA 5005, Australia

(Received 20 November 2013; revised 12 August 2014; accepted 25 August 2014; first published online 19 September 2014)

The first measurement of the influence of the Stokes number on the distributions of particle concentration and velocity at the exit of a long pipe are reported, together with the subsequent influence on the downstream evolution of these distributions through a particle-laden jet in co-flow. The data were obtained by simultaneous particle image velocimetry (PIV) and planar nephelometry (PN), using four cameras to provide high resolution through the first 30 jet diameters and also correction for optical attenuation. These data provide much more detailed information than is available from previous measurements. From them, a new understanding is obtained of how the Stokes number influences the flow at the jet exit plane and how this influence propagates throughout the jet.

Key words: jets, multiphase and particle-laden flows

1. Introduction

Particle-laden turbulent jets, typically consisting of solid particles suspended in a conveying fluid, are an important class of flow not only because of their fundamental significance but also because of their wide relevance to many applications, such as in the flames of boilers and furnaces. The combustion of particle-laden jets typically occurs in the turbulent regime, resulting in complex particle–flow interactions that strongly influence the distributions of both residence time and stoichiometry. These subsequently influence the in-flame distributions of temperature and species concentrations, which in turn influence the key performance characteristics of the flame dimensions, radiant heat transfer and pollutant emissions (Nathan *et al.* 2006). Therefore, an understanding of particle-laden flows is crucial to optimising combustion processes in industrial systems to enable the design of safer, more energy-efficient combustion systems with lower emissions. The significance of these flows has resulted in considerable effort to understand them over the years, with the result that much is now known about particle-laden turbulent jets (Modarress, Tan & Elghobashi 1984*a*; Shuen, Solomon & Zhang 1985; Fleckhaus, Hishida & Maeda 1987; Tsuji *et al.* 1988; Hardalupas, Taylor & Whitelaw 1989; Mostafa *et al.* 1989; Sheen, Jou & Lee 1994; Prevost *et al.* 1996; Fan *et al.* 1997; Frishman *et al.* 1999; Gillandt, Fritsching & Bauckhage 2001). However, the greater complexity of these flows over

†Email address for correspondence: timothy.lau@adelaide.edu.au

their single-phase counterpart, which includes the introduction of many additional parameters together with the many additional experimental challenges introduced both by the conveying fluid and the measurement of particle-laden flows, means that many gaps in understanding persist. The overall aim of the present investigation is to address this gap in understanding through a detailed and systematic experimental investigation of well-characterised, turbulent, particle-laden jets.

The full characterisation of particle-laden turbulent jets requires the simultaneous measurement of the velocity field of both phases, together with the local, instantaneous particle size and number density. Preferably, such measurements should also be performed simultaneously in multiple dimensions and with sufficient spatial and temporal resolution owing to the turbulent nature of the flow. This challenge is so great that all previous experiments of particle-laden jets provide incomplete detail of the flow and/or address only a small number of flow conditions. Additionally, the experiments performed in different laboratories cannot be directly compared, as they have all been performed with different combinations of initial and/or boundary conditions, such as particle size distribution, particle mass loading, co-flow velocity and nozzle geometry. Furthermore, no previous investigation has provided a complete description of the inflow conditions, such as detailed profiles of the mean and fluctuating components of the velocity and scalar fields at the nozzle exit.

The conditions under which previous measurements of the velocity and scalar distributions within particle-laden turbulent jets were performed are shown in table 1. Of the previous measurements of the velocity field (Modarress *et al.* 1984*a*; Shuen *et al.* 1985; Fleckhaus *et al.* 1987; Tsuji *et al.* 1988; Hardalupas *et al.* 1989; Mostafa *et al.* 1989; Sheen *et al.* 1994; Prevost *et al.* 1996; Fan *et al.* 1997; Frishman *et al.* 1999; Gillandt *et al.* 2001), only five (Fleckhaus *et al.* 1987; Tsuji *et al.* 1988; Mostafa *et al.* 1989; Fan *et al.* 1997; Frishman *et al.* 1999) also report the concentration of the dispersed phase. Of these, none report the important Stokes number (Sk_0) range of order unity, in which the particle response time is the same order of magnitude as the fluid time scale, but are instead limited to the range of $Sk_0 > 9$, in which particles exhibit a relatively weak response to turbulent motions. The Stokes number regime of order unity is also particularly relevant in the study of industrial burners, as common flow conditions within these burners, shown in table 2, typically result in a Stokes number of order unity (Smoot & Smith 1985; Mullinger & Jenkins 2008; Nathan *et al.* 2012). Furthermore, out of all the previous experiments, only Mostafa *et al.* (1989) employ a truly mono-disperse particle distribution (using a standard deviation in particle size distribution of less than 5 %), although Fleckhaus *et al.* (1987) and Hardalupas *et al.* (1989) employ particles with a standard deviation of particle size distribution of less than 15 %. A narrow particle size distribution is important, as a wide range of particle sizes can lead to the masking of important details of the influence of the Stokes number, owing to the squared dependence of the Stokes number on particle diameter.

All of the previous measurements of particle-laden turbulent jets have been performed with single-point measurement techniques. Despite their value, such measurements typically cover only a limited region of the flow and are also unable to provide information such as spatial correlations (Liepmann & Gharib 1992) and proper orthogonal decomposition (Bi *et al.* 2003), or to identify particle clusters (Birzer, Kalt & Nathan 2011). In addition, without detailed inflow profiles of velocity and concentration of both the jet and co-flow, none are suitable for detailed model validation. Indeed, the paucity of two-dimensional experimental data in two-phase turbulent flows has been identified as a major impediment to the advancement of

https://doi.org/10.1017/jfm.2014.496 Published online by Cambridge University Press

Reference	Sk_0	Re_D	ϕ	x/D	$\Delta x/D$	$\Delta r/D$	$\widetilde{\sigma}_{dp}$	Method	Measurements performed
Gillandt *et al.* (2001)	>20	5700	1.0	≈0–13	≈1.0	≈0.0625	≈25 %	LDA	$U_p + U_g,\ U_1$
Hardalupas *et al.* (1989)	⩾10	13 000	0.13–0.86	=0–28	≈5	≈0.067	≈15 %	PDA	$U_p,\ U_g,\ U_1$
Modarress *et al.* (1984*a*)	≈13.5	13 300	0.32, 0.85	=0–30	≈10	≈0.056	N/A	LDA	$U_p,\ U_g,\ U_1$
Prevost *et al.* (1996)	≈20	13 100	0.08	≈1–45	≈2	≈0.2	≈35 %	PDA	$U_p + U_g$
Sheen *et al.* (1994)	>180	20 000	0–3.6	≈0–80	≈8	≈0.1	≈10 %	LDA	$U_p,\ U_g,\ U_1$
Shuen *et al.* (1985)	>110	17 000	0.2–0.66	≈0–50	≈5	≈0.2	≈25 %	LDA	$U_p,\ U_g$
Fan *et al.* (1997)	9, 13.6	⩾54 000	0.22, 0.8	≈0–20	≈2	≈0.3	≈35 %	LDA	$U_p,\ U_g,\ U_1,\ \Theta$
Fleckhaus *et al.* (1987)	>71	20 000	0.3	=10–30	N/A	≈0.1	≈25 %	LDA	$U_p + U_g,\ U_1,\ \Theta$
Frishman *et al.* (1999)	11–21	>30 000	0.3–0.62	≈0–65	≈0.25	≈0.2	≈15 %	LDA	$U_p + U_g + \Theta$
Mostafa *et al.* (1989)	≈11–14	5 700	0.2–1.0	=0.6–12	≈3	≈0.125	≈5 %	PDA	$U_p + \Theta,\ U_g$
Tsuji *et al.* (1988)	>120	>14 000	0.55–1.4	≈0–20	≈2.5	≈0.15	N/A	LDA	$U_p,\ U_g,\ U_1,\ \Theta$
Current	0.3, 1.4, 11.2	10 000–20 000	0.4	=0–30	⩽0.134	⩽0.034	⩽5 %	PIV/PN	$U_p + \Theta$

TABLE 1. A summary of previous measurements of the distributions of velocity and/or concentration in particle-laden, turbulent jets. Technique abbreviations: LDA, laser Doppler anemometry; PDA, phase Doppler anemometry; PIV, particle image velocimetry; PN, planar nephelometry. Here, $\widetilde{\sigma}_{dp}$ is the standard deviation of the particle size distribution normalised by the mean particle diameter, U is velocity, Θ is concentration (number density), x is the axial coordinate, r is the radial coordinate, D is the pipe diameter, ϕ is the particle mass loading, N/A = not available and the plus sign refers to simultaneous measurements. Here, Δx and Δr refer to the measurement resolution in the axial and radial directions, respectively, while subscripts p, g and 1 refer to the particle, gas and single phase, respectively.

Particle diameter	50–100 μm
Particle density	1200–1700 kg m^{-3}
Flow velocity	50–100 m s^{-1}
Nozzle diameter (reference)	∼1 m
Resultant exit Stokes number	≈0.2–5.0

TABLE 2. Typical conditions found within industrial direct-fired pulverised coal burners (Smoot & Smith 1985; Mullinger & Jenkins 2008; Nathan *et al.* 2012).

computational fluid dynamic (CFD) models (Fairweather & Hurn 2008; Balachandar & Eaton 2010).

For these reasons, the current research programme, of which the present paper reports the first stage of the campaign, aims to fill these research gaps by providing a comprehensive assessment of both the scalar and velocity fields within a particle-laden jet for a wide range of systematically varied Stokes numbers for mono-disperse particles in the turbulent regime. Specifically, it aims to provide new insight into the role of the Stokes number on the velocity and concentration distributions within a turbulent jet under the three different jet-exit Stokes number regimes, $Sk_0 \ll 1$, $Sk_0 \approx 1$ and $Sk_0 \gg 1$, spanning the exit plane, the near field and into the developed region in which the mean field displays self-similarity.

1.1. *Theory*

In the far field of a turbulent jet, the jet scalar and velocity fields are typically characterised using similarity equations (Rajaratnam 1976). While these equations do not strictly constitute governing equations of the flow, they nonetheless characterise the far field of a turbulent round jet in a zero pressure gradient (Hussein, Capp & George 1994). Under these conditions, the velocity decay in the far field can be expressed as

$$\frac{U_c}{U_e} = K_{1,U}\left(\frac{d_\epsilon}{x - x_{01,U}}\right), \tag{1.1}$$

where U_c is the centreline velocity, U_e is the centreline velocity at the jet exit, d_ϵ is the equivalent diameter, x is the axial coordinate, $K_{1,U}$ is the velocity decay constant and $x_{01,U}$ is the virtual origin associated with the velocity decay. The velocity half-radius (or half-width), $r_{0.5,U}$, can be expressed as

$$\frac{r_{0.5,U}}{d_\epsilon} = K_{2,U}\left(\frac{x - x_{02,U}}{d_\epsilon}\right), \tag{1.2}$$

where r is the radial coordinate, $K_{2,U}$ is the jet spreading (or expansion) constant based on the velocity and $x_{02,U}$ is the virtual origin based on $r_{0.5,U}$. It should be noted that the two virtual origins, $x_{01,U}$ and $x_{02,U}$ are not necessarily equal.

Similarly, the centreline concentration (particle number density) and concentration half-width can be expressed, respectively, as

$$\frac{\Theta_c}{\Theta_e} = K_{1,\Theta}\left(\frac{d_\epsilon}{x - x_{01,\Theta}}\right) \tag{1.3}$$

and

$$\frac{r_{0.5,\Theta}}{d_\epsilon} = K_{2,\Theta}\left(\frac{x - x_{02,\Theta}}{d_\epsilon}\right), \tag{1.4}$$

where Θ_c is the centreline concentration, Θ_e is the centreline concentration at the jet exit, $K_{1,\Theta}$ is the concentration decay constant, $K_{2,\Theta}$ is the jet spreading constant based on the concentration, $x_{01,\Theta}$ is the virtual origin associated with the concentration decay profile and $x_{02,\Theta}$ is the virtual origin based on the concentration half-width profile.

The preferred equivalent diameter is the momentum diameter, defined as (Thring & Newby 1953)

$$d_\epsilon = 2\sqrt{\frac{\rho_j}{\rho_\infty}}\left[\frac{2\displaystyle\int_0^{D/2} U_{g,ex}(r)\, r\,\mathrm{d}r}{\sqrt{2\displaystyle\int_0^{D/2} U_{g,ex}^2(r)\, r\,\mathrm{d}r}}\right], \tag{1.5}$$

where ρ_j and ρ_∞ are the density of the particle-laden jet and co-flow, respectively, $U_{g,ex}(r)$ is the gas-phase velocity profile at the pipe exit and D is the pipe diameter. The equivalent diameter accounts for differences in initial density ratio and exit velocity profile. Here, the distribution $U_{g,ex}(r)$ was approximated to be that of the single-phase velocity at the same Reynolds number, which was measured using hot-wire anemometry (HWA) (see also § 2.3). The jet density was based on the bulk value of the particle–air mixture, leading to a density ratio of $\rho_j/\rho_\infty = 1 + \phi$, where ϕ is the particle mass loading, defined as the ratio of the particle-to-air mass flow rate.

Finally, the reference bulk-mean velocity, U_b and bulk-mean concentration, Θ_b, is defined as follows:

$$U_b = \frac{8}{D^2}\int_0^{D/2} U_{g,ex}(r)\, r\,\mathrm{d}r \tag{1.6}$$

$$\Theta_b = \frac{8}{D^2 U_b}\int_0^{D/2} \Theta_{ex}(r)\, U_{p,ex}(r)\, r\,\mathrm{d}r \tag{1.7}$$

where Θ_{ex} and $U_{p,ex}$ are the particle concentration and axial velocity at the pipe exit, respectively.

2. The experimental arrangement

Simultaneous digital particle image velocimetry (PIV) and planar nephelometry (PN) were performed in a turbulent jet of air seeded with solid, spherical particles surrounded by a co-flow and contained within a low-confinement wind tunnel. The jet was generated by a compressed air source, delivered through a long, round stainless steel pipe. The particle-laden fluid was introduced into the long pipe using two diametrically opposed circular inlets at right angles to the pipe (see figure 1). This configuration was found to assist in achieving symmetry in the exit distributions of concentration and velocity.

The experiment was performed using a pipe with a diameter $D = 12.7$ mm and a length of $L = 2080$ mm, corresponding to a length-to-diameter ratio of $L/D \approx 163.8$. For single-phase turbulent jets, this is sufficient to generate a fully developed pipe flow (Rajaratnam 1976); however, the required length to establish fully developed particle-laden flows has not been reported. To ascertain whether $L/D \approx 163.8$ was sufficient to establish a fully developed particle-laden pipe flow, the experiments were repeated with identical Stokes numbers, utilising a similar pipe with a diameter $D = 9.525$ mm and a length of $L = 2870$ mm, leading to $L/D \approx 301.3$. The concentration and velocity

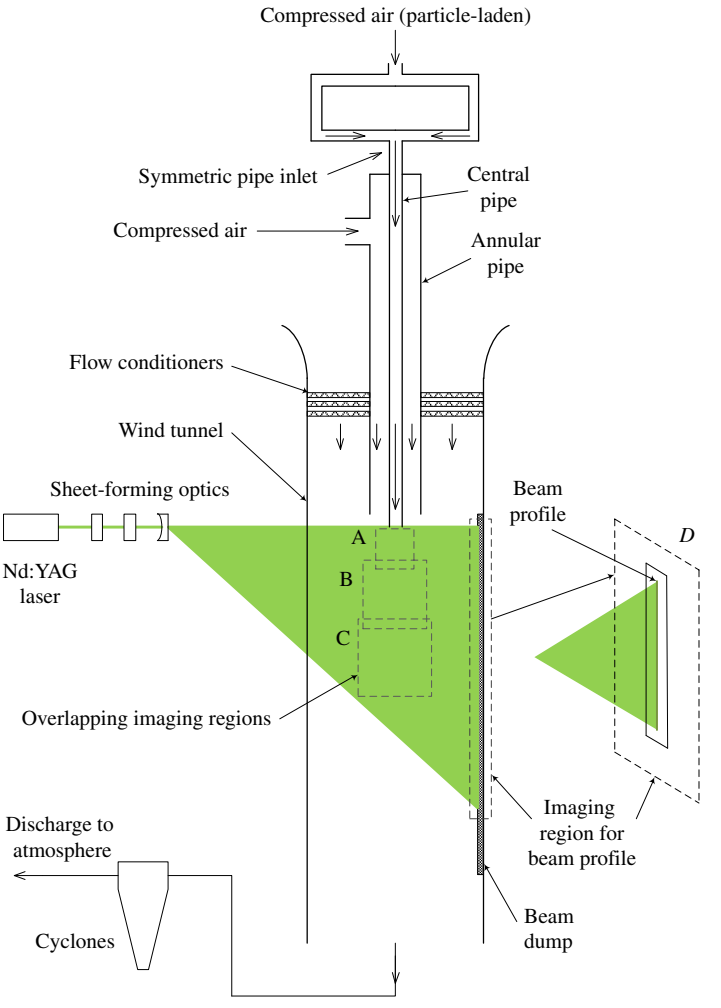

FIGURE 1. (Colour online) The experimental arrangement.

profiles at the pipe exit were found to have closely converged for both L/D ratios at all investigated Stokes numbers, indicating that $L/D \approx 163.8$ is sufficiently long to closely approximate a fully developed particle-laden pipe flow (see the Appendix). As the larger, shorter pipe ($L/D \approx 163.8$) results in higher Reynolds numbers and allows for better data resolution than the smaller pipe, this case was selected as the primary case for analysis in this paper.

The central pipe was positioned concentrically within a larger annular pipe of diameter $D_a = 69.0$ mm, the exit plane of which was positioned 60.0 mm upstream from the exit plane of the central nozzle. Both the annular and central pipes were mounted vertically in an open loop wind tunnel, as shown in figure 1, to avoid gravity bias. The purpose of the co-annular jet is to provide the means to seed only the inner region of the co-flow with tracer particles, to allow the measurement of the co-flow velocity without polluting the windows of the tunnel. However, this facility was not used in the current experiments because measurement of the co-flow velocity

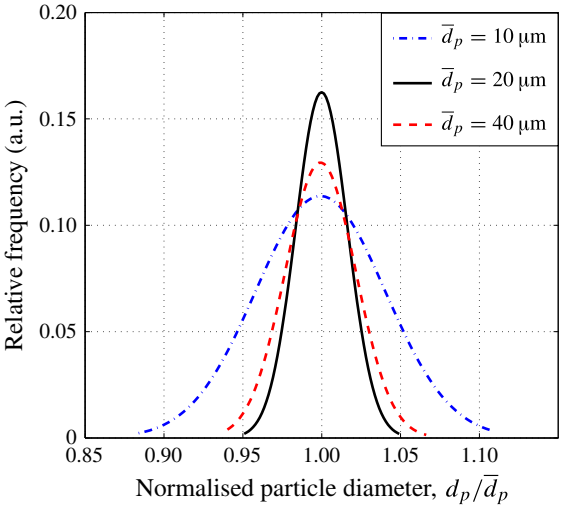

FIGURE 2. (Colour online) The particle size distribution.

is not reported and, moreover, the use of tracers would contaminate the measurement of both the particle velocity and concentration.

The velocity of the co-annular jet was matched to within $\pm 5\,\%$ of the velocity of the wind tunnel, leading to an approximately uniform co-flow across the wind tunnel to the walls of the central pipe. Both central and annular pipes, together with all associated fittings, were electrically grounded to avoid any build-up of static charge.

The wind tunnel has a cross-section of 650 mm $\times$ 650 mm. The axial distance from the jet exit plane to the downstream end of the tunnel was 1000 mm, while the distance from the centre of the jet to the sidewalls of the tunnel was 325 mm. The maximum width of the jet was approximately 30 mm (measured from the jet centreline) at the end of the measurement region, making the jet free from wall effects within the working section. The ratio of the jet-to-co-flow velocity was fixed at 12.0:1.

The central jet was laden with solid polymer spheres (Microbeads Spheromers) of mean diameter $\overline{d}_p = 10$, 20 and 40 μm, and a standard deviation of $\tilde{\sigma}_{dp} \leqslant 5\,\%$ (see figure 2). The narrow size distribution was central to their selection, making the size distribution truly mono-disperse and avoiding the need to measure the particle size *in situ*. The density of the particles is $\rho_p = 1200$ kg m^{-3}. The particle mass loading was fixed at $\phi = 0.4$. This is sufficiently high for the particles to exert a significant influence on the surrounding fluid, while being sufficiently low for particle-to-particle interactions to be small, i.e. the particle–fluid interaction is within the two-way coupling regime (Elghobashi 2006).

The flow conditions were selected to result in at least one case in each Stokes regime, while also maintaining a sufficiently high Reynolds number ($Re_D \gtrsim 10\,000$) to ensure fully turbulent flow. This resulted in three cases of exit Stokes number ranging across two orders of magnitude, i.e. $Sk_0 = 0.3$, 1.4 and 11.2, which were obtained using three particle diameters and two jet velocities, as shown in table 3. This results in jet-exit Reynolds numbers of $Re_D = 10\,000$ and $Re_D = 20\,000$. Here, the jet-exit Stokes number is defined as

$$Sk_0 = \frac{\rho_p \overline{d}_p^2 U_b}{18 \mu D} \tag{2.1}$$

Exit Stokes number, Sk_0	Mean particle diameter, $\overline{d}_p$ (μm)	Jet bulk velocity, U_b (m s^{-1})	Exit Reynolds number, Re_D
0.3	10	12	10 000
1.4	20	12	10 000
11.2	40	24	20 000

TABLE 3. A summary of the experimental parameters. The pipe diameter is $D = 12.7$ mm.

Camera	Array size (pixels)	Bit depth	Axial imaging extent (mm)	PIV IW size (pixels)	Probe volume, velocity (mm)	Probe volume, concentration (μm)
A	1018 × 1008	10 bit	0–51	8 × 64	1.60 × 0.20 × 0.35	50.1 × 50.1 × 350
B	1920 × 1080	12 bit	40–240	8 × 32	1.67 × 0.42 × 0.35	104.2 × 104.2 × 350
C	1600 × 1200	12 bit	230–400	8 × 32	1.70 × 0.43 × 0.35	106.3 × 106.3 × 350
D	1018 × 1008	10 bit	0–510	—	—	—

TABLE 4. Details of the imaging system. The axial imaging extent was measured from the jet exit, and the length components are radial × axial × normal.

while the exit Reynolds number is defined as

$$Re_D = \frac{\rho_a U_b D}{\mu}, \tag{2.2}$$

where μ and ρ_a are the viscosity and density of air, respectively. Single-phase measurements are denoted as $Sk_0 = 0$.

2.1. *Particle image velocimetry*

The velocity of the dispersed phase in the particle-laden jet was measured using digital PIV (Raffel, Willert & Kompenhans 1998). The source of illumination was a double-head, pulsed Nd:YAG laser (Quantel Brilliant B) with a fixed pulsing frequency of 10 Hz and a maximum power of approximately 300 mJ per pulse. The laser was operated in the frequency-doubled mode at 532 nm. The laser beam was formed into a diverging sheet that was aligned with the nozzle axis and positioned to illuminate all of the exit plane, as shown in figure 1. The thickness of the light sheet was estimated to be $\approx 350 \pm 50$ μm, based on measurements of laser burn marks on light-sensitive paper made under a microscope.

Images were captured simultaneously from four separate Kodak Megaplus cameras. Three cameras were used to capture different downstream locations, while the fourth camera was used to record the beam profile transmitted through the particle-laden jet (see figure 1). The characteristics of the imaging region, the resolution and the resultant probe volume for each individual camera are summarised in table 4. Each flow condition was recorded over four separate realisations, with each realisation lasting approximately 120 s. Given that the minimum jet velocity used in the experiment is $U_b = 12$ m s^{-1}, and assuming that the length scale of a large eddy is approximately the size of the pipe diameter, each experimental realisation corresponds to more than 10^5 convection times of a large eddy. This sampling period was deemed to be sufficient to capture the long time scale motions in the flow. A minimum of

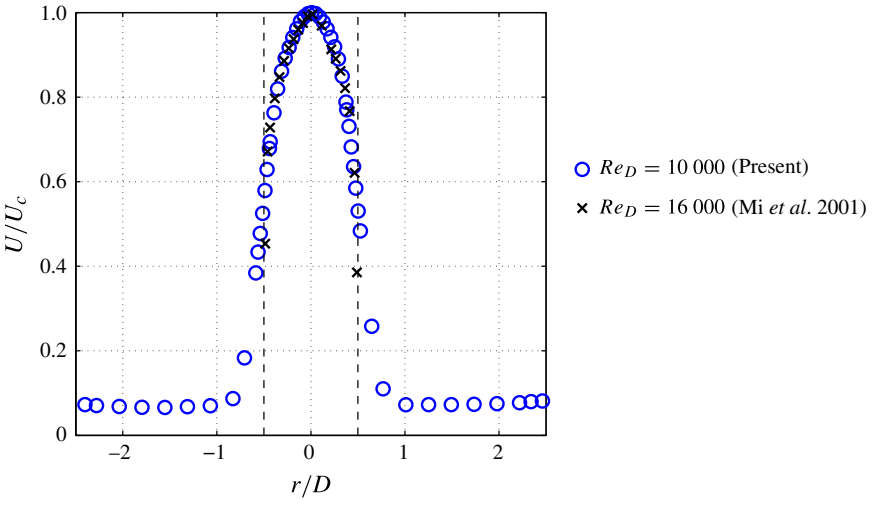

FIGURE 3. (Colour online) The single-phase mean axial velocity at the jet exit as recorded by HWA, both for the present jet with co-flow and for a previous jet without co-flow.

1280 images was recorded by each camera for each realisation. Images were processed utilising the command-line interface of PIVView 2.1. The PIV interrogation window (IW) size for each imaging region is also shown in table 4. In all cases, a 50 % overlap was used. Outliers were detected using an in-house code based on both absolute velocity and relative velocity difference. All spurious vectors were removed from the analysis.

2.2. *Planar nephelometry*

The scalar field was measured using PN, which infers the relative particle number density (i.e. concentration) from the intensity of the measured Mie scattering signal (Birzer, Kalt & Nathan 2012). The same images collected for the PIV measurements (§ 2.1) were also used for the PN measurement. Each image was corrected for beam profile using the profile associated with the appropriate laser head, and beam attenuation on a shot-by-shot basis using an iterative correction scheme that references transmitted light recorded by the beam profiler, following our earlier work (Kalt, Birzer & Nathan 2007; Kalt & Nathan 2007).

2.3. *Single-phase jet-exit conditions*

Separate measurements of the single-phase fluid velocity at the jet exit were also performed using HWA. These measurements were performed with identical experimental apparatus and flow conditions as the two-phase experiments, with the exception that the jet was not laden with particles. These measurements were made across both the co-flow and jet, at a single axial location close to the pipe exit ($x/D \approx 0.2$). The mean and root mean square (r.m.s.) axial velocities for the single-phase case at $Re_D = 10\,000$ are shown in figures 3 and 4, respectively. Also shown are the measurements of Mi, Nobes & Nathan (2001) for a similar turbulent, round jet, also issuing from a long pipe but without a co-flow. The good agreement between these two datasets confirms that the inflow conditions to the pipe, combined

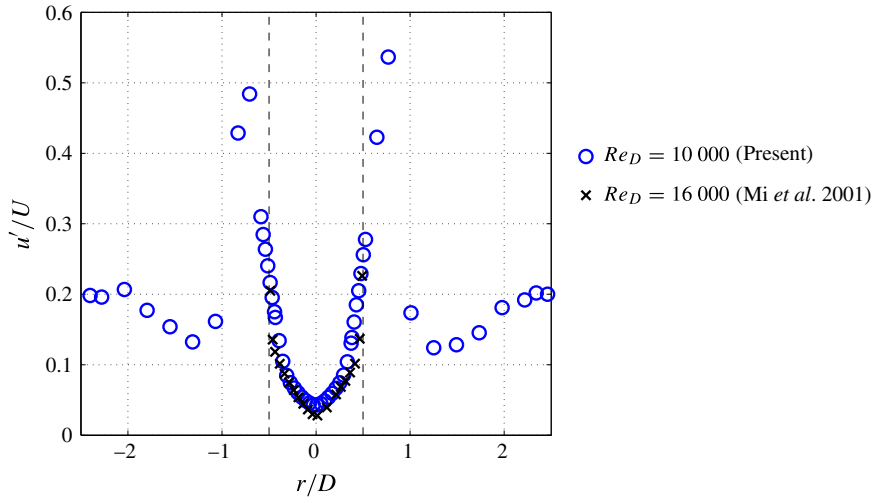

FIGURE 4. (Colour online) The single-phase r.m.s. axial velocity at the jet exit as recorded by HWA, both for the present jet with co-flow and for a previous jet without co-flow.

with its length, are sufficient to achieve fully developed turbulent pipe flow at the pipe exit. Further evidence for this is found from the value of the exponent in the power law for these data, as described in the following equation:

$$\frac{U}{U_c} = \left(1 - \frac{2r}{D}\right)^{1/n}. \tag{2.3}$$

The value of the exponent in the present single-phase jet is $n = 6.0$, which is close to the value $n = 6.5$ reported by Mi *et al.* and to the theoretical value of $n = 7$ for fully developed turbulent pipe flow (Yamaguchi 2008).

3. Results

3.1. *Jet exit profiles*

The mean velocity profile of the particles at the jet exit for all three investigated Stokes numbers is shown in figure 5. The velocity profiles of all three cases conform reasonably closely to each other, with the exponent n (see (2.3)) exhibiting a dependence on the Stokes number, so that $n = 6.3$, 6.6 and 10.4 for $Sk_0 = 0.3$, 1.4 and 11.2, respectively. This compares with the typical value of $n \approx 6.6$ found for the gas phase in similar particle-laden jets (Modarress *et al.* 1984*a*; Fan *et al.* 1997). The increased departure from the single phase with increasing Stokes number is expected, with the highest case, $Sk_0 = 11.2$, tending most towards a top-hat profile, consistent with previous observations that particle velocity profiles of high Stokes number turbulent pipe flows approach a top-hat profile (Modarress, Wuerer & Elghobashi 1984*b*; Tsuji *et al.* 1988; Hardalupas *et al.* 1989; Sheen *et al.* 1994). The close match of the exponent n to the single-phase case for the lower Stokes number cases, together with the trends in the profile, gives further confidence that the development length of the pipe is sufficient for the mean velocity field of the two-phase flow at the exit plane to closely approach the fully developed state.

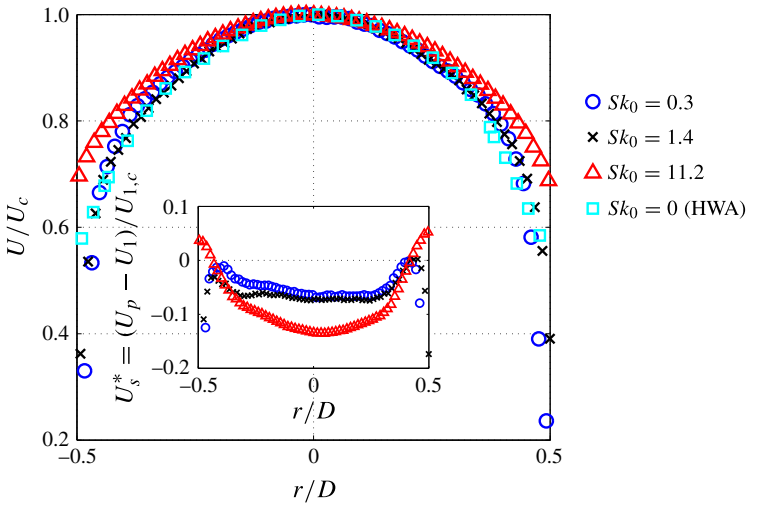

FIGURE 5. (Colour online) Radial profiles of the mean axial velocity at the jet exit. The inset shows radial profiles of the quasi-slip velocity, U_s^*, which is the difference between the axial components of the single-phase gas velocity and the particle velocity. The single-phase ($Sk_0 = 0$) measurements were performed with HWA at $Re_D = 10\,000$. For the flow conditions of the two-phase measurements, see table 3.

The inset to figure 5 presents the radial profiles of the quasi-slip velocity, $U_s^* = \left(U_p - U_1\right)/U_{1,c}$, which is the difference between the two-phase particle velocity and the single-phase gas velocity. Here, U_p is the particle-phase velocity, U_1 is the single-phase velocity and $U_{1,c}$ is the centreline velocity of the single-phase case. The quasi-slip velocity will overestimate the actual slip velocity, since all the investigated two-phase cases are in the two-way coupling regime, where the particles modify the flow velocity towards the particle velocity. Nevertheless, the radial profiles of U_s^* provide useful information. The measurements of U_s^* show that the particles lag the fluid throughout the jet exit for the two lower Sk_0 cases, while for the $Sk_0 = 11.2$ case, the particles lag the fluid for most of the jet exit except near to the jet edge, and also exhibit the highest centreline particle lag, consistent with previous measurements (Hardalupas *et al.* 1989; Gillandt *et al.* 2001).

The r.m.s. value of the normalised axial particle velocity at the jet exit, u'/U, is presented in figure 6. It can be seen that the particle axial r.m.s. velocity distribution is 'U-shaped', with a minimum close to the centre of the jet and a maximum towards the edge of the jet for all Stokes numbers. This result is in broad agreement with the current single-phase measurements, also shown in figure 6, and similar two-phase measurements by Hardalupas *et al.* (1989) and Gillandt *et al.* (2001). The r.m.s. measurements also broadly show that the particle axial velocity fluctuation at the jet exit decreases with increasing Stokes number, consistent with previous studies (Hardalupas *et al.* 1989). The minimum r.m.s. value of the axial velocity is $u'/U = 6.74\,\%$, $4.91\,\%$ and $1.76\,\%$ for $Sk_0 = 0.3$, 1.4 and 11.2, respectively.

Figure 7 presents the mean radial concentration profile at the jet exit for all three Stokes regimes. It can be seen that the scalar field exhibits a much stronger dependence on Sk_0 than does the velocity field. The radial concentration profiles for the two lower Stokes number cases are preferentially distributed towards the outer

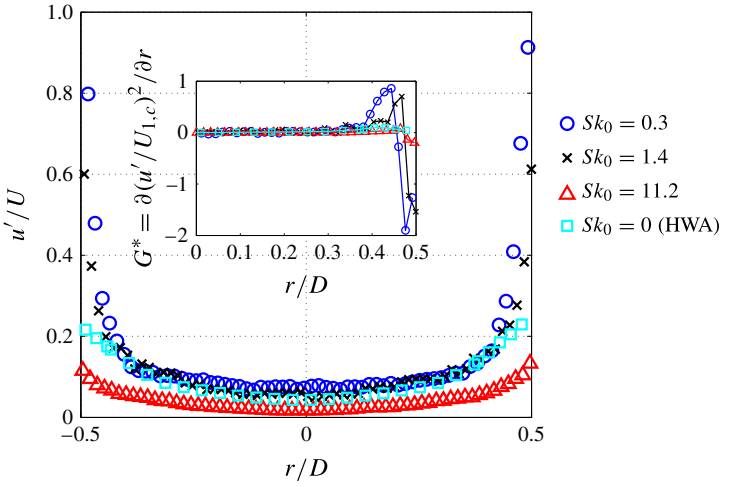

FIGURE 6. (Colour online) Radial profiles of the normalised r.m.s. value of the axial velocity (u'/U) measured at the jet exit. The inset presents the radial gradient of the square of the normalised r.m.s. axial velocity, G^*, at the jet exit. The single-phase ($Sk_0 = 0$) measurements were performed with HWA at $Re_D = 10\,000$. For the flow conditions of the two-phase measurements, see table 3.

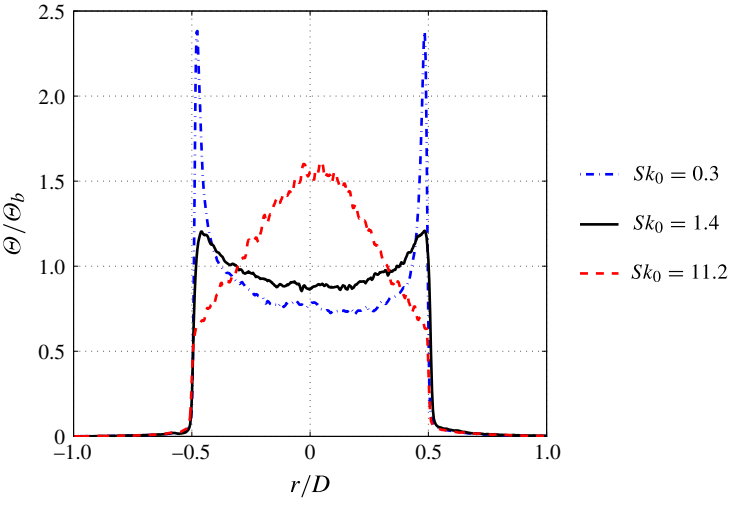

FIGURE 7. (Colour online) The radial concentration profile at the jet exit.

edges of the emerging jet, with the $Sk_0 = 0.3$ case being strongly so. The central core of the jet exhibits a 'U-shaped' concentration profile, with the lowest concentration occurring at the centre. In contrast, the exit concentration profile of the $Sk_0 = 11.2$ case exhibits a 'Λ-shaped' profile, with a maximum at the jet centre and a near-linear decrease with radial distance to the edges of the jet. This latter profile shows broad agreement with other measurements showing higher exit particle concentrations at the axis for high Stokes number particle-laden jets (Tsuji *et al.* 1988; Fan *et al.* 1997). However, the low resolution of these measurements ($0.15 \lesssim \Delta r/D \lesssim 0.3$) makes a

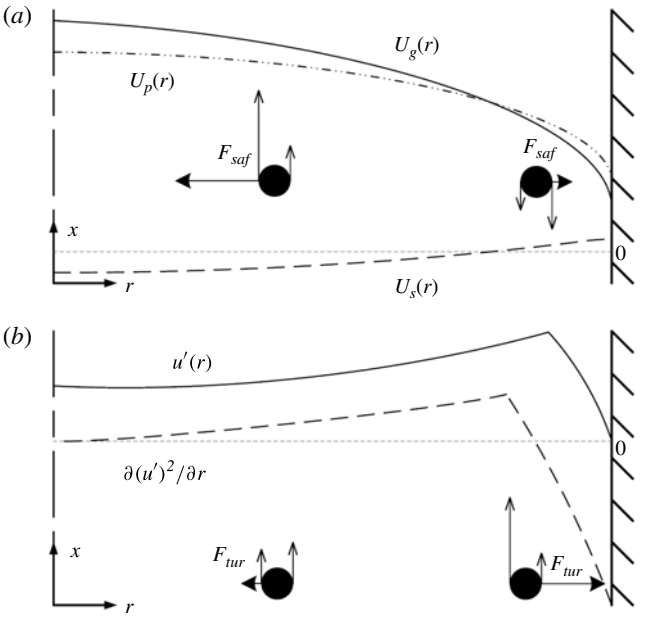

FIGURE 8. Schematic diagrams of (*a*) Saffman lift and (*b*) turbophoresis acting on particles in a fully developed pipe flow. Here, F_{saf} is the Saffman lift force, F_{tur} is the turbophoretic force and $U_s = U_p - U_g$ is the particle slip velocity. The diagram is not to scale (proportions exaggerated for clarity).

direct comparison of exit profiles with the present measurements ($\Delta r/D \leqslant 0.034$) difficult (see table 1).

To the authors' knowledge, the observation that the exit concentration profile switches from a 'U-shaped' to a 'Λ-shaped' profile as Sk_0 is increased from the low to the high regime has not previously been reported. It is postulated that this can be explained by the influence of two forces, namely the Saffman lift force (Saffman 1965; McLaughlin 1991, 1993; Asmolov 1999), and the turbophoretic force (Reeks 1983; Young & Leeming 1997), the relative significance of which is a function of the Stokes number, and the effect of the particle axial acceleration upstream of the pipe exit.

The Saffman lift force, F_{saf}, is a force exerted on a particle due to the presence of a velocity gradient across that particle. For particles lagging the surrounding fluid (i.e. slip velocity $U_s < 0$), the Saffman lift force causes particles to migrate towards regions of high fluid velocity, i.e. towards the pipe axis (see figure 8*a*). Conversely, for particles leading the surrounding fluid, Saffman lift causes particles to migrate towards the pipe boundary. For any given fluid velocity gradient, the magnitude of the Saffman lift force is proportional to the magnitude of the slip velocity (Saffman 1965). Since the magnitude of the slip velocity increases with Stokes number, and since particles lag the fluid in the pipe except close to the pipe wall (see the inset of figure 5), Saffman lift is deduced to dominate in the central region of the pipe when the Stokes number is large, leading to a 'Λ-shaped' concentration profile for the $Sk_0 = 11.2$ case. In the region close to the pipe boundary for the high Stokes number case, the magnitude of the slip velocity, and hence the Saffman lift, is expected to be relatively low.

Turbophoresis is a force induced by inhomogeneous turbulence on particles, which acts in the direction of decreasing particle turbulent kinetic energy (Reeks 1983; Young & Leeming 1997). The magnitude of this turbophoretic force, F_{tur}, is proportional to the gradient of the particle turbulent kinetic energy, and can be estimated from the pseudo-gradient $G^* = \partial(u'/U_{1,c})^2/\partial r$, leading to $F_{tur} \sim -G^*$. The radial profiles of G^* for all three Stokes numbers and the single-phase case is shown in the inset of figure 6. For the highest Stokes number case, $Sk_0 = 11.2$, G^* is small throughout the jet exit, due to the low response of the particles to turbulent fluctuations in the flow. For the two lower Stokes number cases, $Sk_0 = 0.3$ and $Sk_0 = 1.4$, the gradient G^* is small throughout the central region of the jet ($0 \leqslant r/D \lesssim 0.4$). Closer to the jet edge, in the region $0.4 \lesssim r/D \lesssim 0.48$, G^* has a positive value, while very close to the wall, it is strongly negative. The strong negative values close to the wall are due to the damping of turbulent fluctuations by the wall, which are underestimated by the values of G^*, because the measurement plane is downstream from the exit plane, where fluctuations at the jet edge are greater than that close to the wall within the pipe. Nevertheless, this measurement of a high magnitude, negative G^* in a thin, near-wall region, followed by a low-magnitude, positive gradient G^* just outside of this near-wall region, is also consistent with previous single-phase measurements of turbulent pipe and channel flows (Kim, Moin & Moser 1987; Eggels *et al.* 1994; Kussin & Sommerfeld 2002). Therefore, in the near-wall region of the pipe at low Stokes numbers, turbophoresis is deduced to exert a significant force towards the wall, causing particles to migrate towards the pipe boundary (as illustrated in figure 8*b*). The effect of turbophoresis is particularly evident for the lowest Stokes number case, $Sk_0 = 0.3$, resulting in a narrow region of high concentration at $r/D \approx \pm 0.5$. Outside this near-wall region, the turbophoretic force causes particles to migrate towards the axis, although this force is less significant. For particles with high Stokes numbers, turbophoresis is estimated to be small.

In the central region of the jet ($0 \leqslant r/D \lesssim 0.4$), the influence of both Saffman lift and turbophoresis is expected to be weak for the two lower Stokes number cases. Therefore, in these regions, lateral particle migration is predicted to be small. Under these conditions, the particle-phase continuity equation is

$$\frac{\partial \Theta U_p}{\partial x} + \frac{1}{r}\frac{\partial r \Theta V_p}{\partial r} = 0, \tag{3.1}$$

where V_p is the radial velocity of the particles. In addition, where the radial velocity of the particles, $V_p \approx 0$, it can be shown that $\Theta(r, x)\, U_p(r, x) \approx \Theta_0(r)\, U_{p,0}(r)$, where Θ_0 and $U_{p,0}$ are the particle concentration and axial velocity at the beginning of the pipe, respectively. That is, the axial acceleration of the flow in the upstream region of the pipe in which the fully developed two-phase boundary layer is established leads, by continuity, to a particle concentration profile that tends towards being inversely proportional to the velocity profile. Since the current particle velocity profiles are '$\cap$-shaped' (as shown in figure 5), in the absence of any other significant forces the concentration profiles tend to become 'U-shaped'.

Therefore, the measured exit concentration profiles for all investigated Stokes numbers (figure 7) can then be broadly explained in terms of the relative significance of Saffman lift, turbophoresis and the effect of particle axial acceleration within the flow development region of the pipe. For particles with a high Stokes number in the central region of the pipe, Saffman lift is significant, causing particles to migrate towards the pipe axis and resulting in a 'Λ-shaped' radial particle concentration

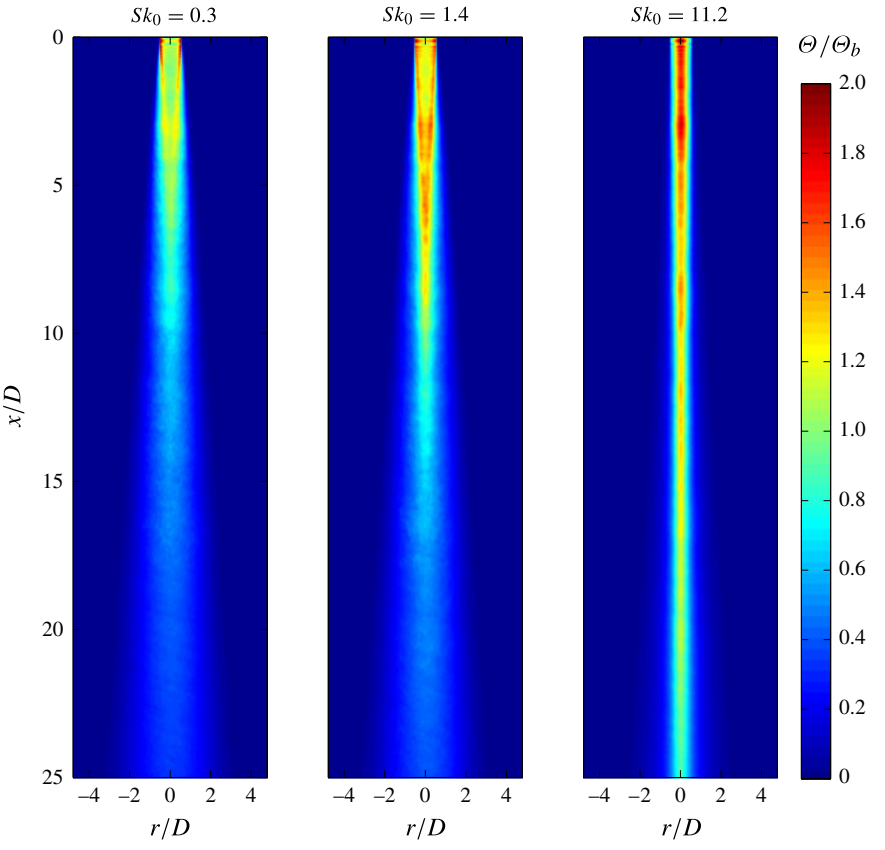

FIGURE 9. (Colour online) The mean distributions of particle concentration normalised by the bulk-mean exit values (Θ/Θ_b) for three values of Sk_0.

profile. For particles with a low Stokes number in the near-wall region of the pipe, turbophoresis dominates, causing particles to migrate towards the pipe boundary, resulting in narrow regions of high concentration at $r/D \approx \pm 0.5$. In the central region of the jet ($0 \leqslant r/D \lesssim 0.4$) for the two lower Stokes numbers, Saffman lift and turbophoresis are both weak, and the 'U-shaped' concentration profile is a result of axial particle acceleration in the flow development region far upstream of the pipe exit.

While the measurements reported herein (figures 5–7) provide strong evidence to support this explanation, additional highly resolved, simultaneous measurements (or DNS calculations) of the gas- and particle-phase velocity, particularly within, and in the near-wall region, of the pipe are required to confirm this.

3.2. *The concentration field*

Figure 9 presents the normalised two-dimensional particle concentration (number density) field, Θ/Θ_b, of the jet for all three Stokes numbers investigated. The dramatic differences of the exit concentration as a function of the Stokes number, as described above, are seen to significantly influence the entire near field of the jets. That is, for the cases $Sk_0 = 0.3$ and 1.4, the particles, which leave the pipe

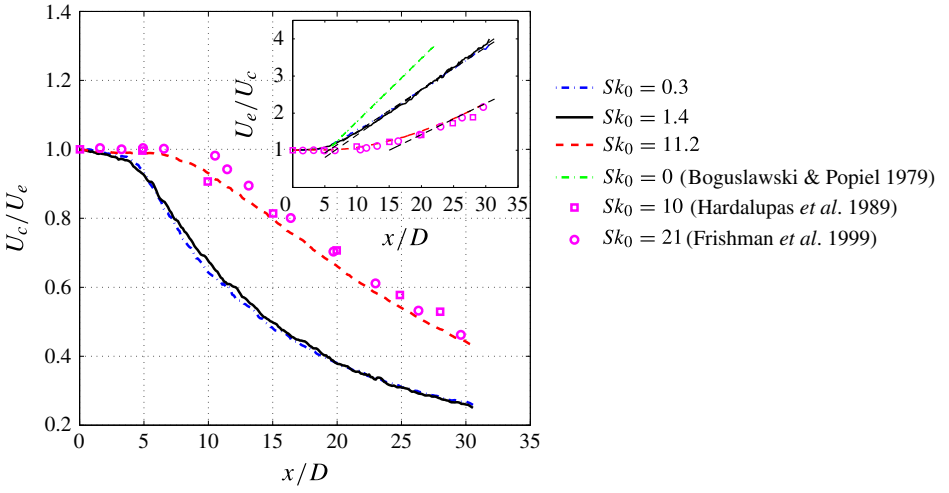

FIGURE 10. (Colour online) The axial evolution of the centreline velocity decay. The inset shows the axial evolution of the inverse centreline velocity.

preferentially distributed towards the edge of the jet, start migrating towards the jet axis beyond $x/D \approx 0.5$, such that they remain near the jet edge through most of the near-field region, until they fully converge to the jet axis at $x/D \approx 4$. This is in stark contrast to the high Stokes number case, in which the particles are preferentially concentrated on the axis right from the exit plane. This near-field influence can be deduced to augment the already well-known trend, which is also evident here, in which the rates of spread and streamwise decay of a turbulent jet decrease with an increase in the Stokes number (Hardalupas *et al.* 1989; Mostafa *et al.* 1989; Prevost *et al.* 1996; Fan *et al.* 1997). The well-known explanation for this is that the inertia of the particles relative to the gas phase increases with Sk_0 (Balachandar & Eaton 2010).

3.3. *Jet decay*

Figure 10 presents the centreline velocity decay of the jet for all three Stokes numbers. The $Sk_0 = 0.3$ and $Sk_0 = 1.4$ cases exhibit a very similar jet-decay profile to each other, with a low rate of decay through the 'potential core' of length 4–5 pipe diameters, followed by a region that converges to a decay rate that scales with x^{-1}. Here, the term 'potential core' is used in inverted commas because a pipe jet does not exhibit a true potential core (being without a core of fluid of uniform velocity), but instead it refers to the region of the jet where the centreline velocity or concentration does not decrease with axial distance. The jet-decay trends are more clearly illustrated in the inset of figure 10, which shows the inverse of the centreline velocity decay. The inverse decay is linear for $x/D \gtrsim 7$. The corresponding velocity decay coefficients are $K_{1,U} = 7.43$ and $K_{1,U} = 6.95$, while the velocity decay virtual origins are $x_{01,U}/d_\epsilon = -2.69$ and $x_{01,U}/d_\epsilon = -1.37$ for $Sk_0 = 0.3$ and $Sk_0 = 1.4$, respectively (see also (1.1)). The velocity decay coefficients measured here for low Stokes numbers are slightly higher than the values of $K_{1,U} = 5.9$ (Boguslawski & Popiel (1979), shown in the inset of figure 10) and $K_{1,U} = 6.5$ (Xu & Antonia 2002) found in previous measurements of single-phase jets issuing from a long pipe, implying that the current two-phase jet

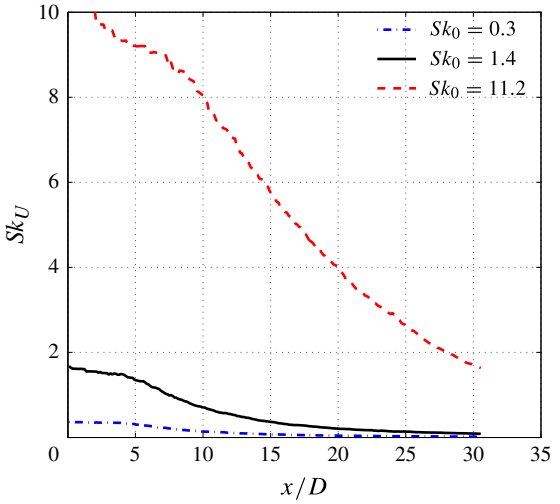

FIGURE 11. (Colour online) Variation of the local Stokes number with streamwise distance from the jet exit.

has a lower velocity decay rate than similar single-phase jets. This may be attributed to the known trend that particles decrease the spreading rate of a jet (Modarress *et al.* 1984*a*; Shuen *et al.* 1985; Hardalupas *et al.* 1989; Mostafa *et al.* 1989; Sheen *et al.* 1994; Prevost *et al.* 1996; Fan *et al.* 1997). Additionally, this may also be attributed to the influence of the present jets being in a low-velocity co-flow, while the single-phase jets discussed above were unconfined. While the effect of co-flow is expected to be small in the near field for co-flow velocities less than 20 % of the jet velocity (Antonia & Bilger 1973), in the far field a co-flow does decrease the decay rate of a jet.

Figure 10 also shows that the $Sk_0 = 11.2$ case exhibits a longer 'potential core', and a lower rate of centreline decay than the lower Stokes number cases, consistent with previous observations (Prevost *et al.* 1996). However, the centreline decay rate of the particle velocity scales more closely with x (with a negative gradient) than with x^{-1} over this measurement range, consistent with measurements at similar high Stokes numbers by Hardalupas *et al.* (1989) ($Sk_0 = 10$, $\phi = 0.8$) and Frishman *et al.* (1999) ($Sk_0 = 21$, $\phi = 0.62$), which are also shown in the figures. The most likely explanation for the departure of the centreline velocity decay from the expected x^{-1} profile can be found from the axial evolution of the local Stokes number, defined as

$$Sk_U = \frac{\rho_p \overline{d}_p^2 U_c}{36\mu r_{0.5,U}} \approx Sk_0 \left(\frac{D/2}{r_{0.5,U}}\right)\left(\frac{U_c}{U_e}\right). \tag{3.2}$$

The axial evolution of the local Stokes number is shown in figure 11. This figure shows that, for the $Sk_0 = 11.2$ case, Sk_U exhibits a gradual transition from order 10 at the exit plane, in which the particles are unresponsive to dominant eddies, to order unity at the end of the measurement regime, where they exhibit a partial response to the flow. This is consistent with the inverse velocity decay rate undergoing a gradual increase through the measurement region and transitioning towards a constant value by the end of the region. An estimate of the far-field decay rate is obtained by fitting a linear curve to the inverse velocity decay data for $x/D \gtrsim 25$, as shown in the inset of

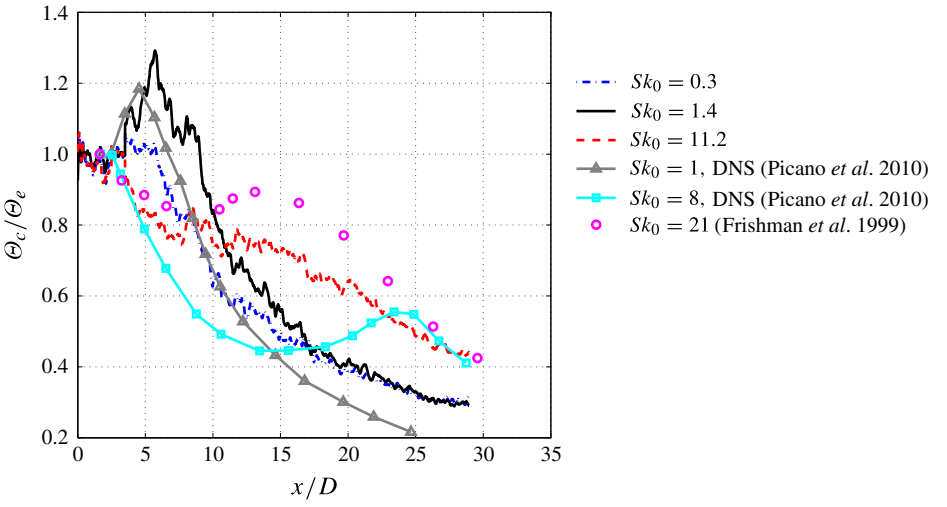

FIGURE 12. (Colour online) The axial evolution of the centreline concentration decay.

figure 10, which yields $K_{1,U} \approx 10.03$ and $x_{01}/d_\epsilon \approx 2.63$. The velocity decay coefficient obtained here is comparable with the value of $K_{1,U} = 10.5$ measured previously in a particle-laden jet at the similar conditions of $Sk_0 = 13.5$ and $Re_D = 13\,000$ (Modarress *et al.* 1984*a*).

The centreline concentration decay of the jet for all three Stokes numbers, smoothed using a five-point moving average filter to improve clarity, is shown in figure 12. In all three cases, this concentration is constant through the first two and a half diameters of the 'potential core'. For the two lower Stokes number cases, the centreline concentration exhibits a near-field hump in the centreline concentration, in which the centreline concentration is increased above the exit value by the migration of particles from the edges of the jet towards the jet axis, consistent with the planar images shown in figure 9. The presence of a near-field hump in the centreline particle concentration for flows with low Sk_0 but not for cases with high Sk_0 is consistent with previous experimental measurements (Laats & Frishman 1970). However, the important role of the upstream flow within the pipe in generating this hump through the redistribution of the radial profiles as a result of the influence of Sk_0 on the exit profiles has not been reported previously.

The centreline concentration decay for the $Sk_0 = 1.4$ case is also broadly consistent with recent direct numerical simulations (DNS) of a particle-laden jet at the similar exit Stokes number of $Sk_0 = 1.0$ (Picano *et al.* 2010), although the modelled results do not exhibit a truly linear inverse decay in the far field, as illustrated in figure 13. Additionally, the inverse decay rate of the $Sk_0 = 1.0$ case calculated with DNS is much more similar to the single-phase case than to the present $Sk_0 = 1.4$ case, consistent with its operation in the one-way coupling regime, while the present measurements were recorded in the two-way coupling regime. The results of the same DNS at $Sk_0 = 8.0$ are markedly different from the current experimental measurements at $Sk_0 = 11.2$, with the DNS indicating a hump in the centreline concentration at $x/D \approx 24$. In contrast, the experimental results do not show any increase in the centreline concentration for the entire measurement region ($x/D < 30$) for the $Sk_0 = 11.2$ case. This apparent discrepancy is attributed primarily to the

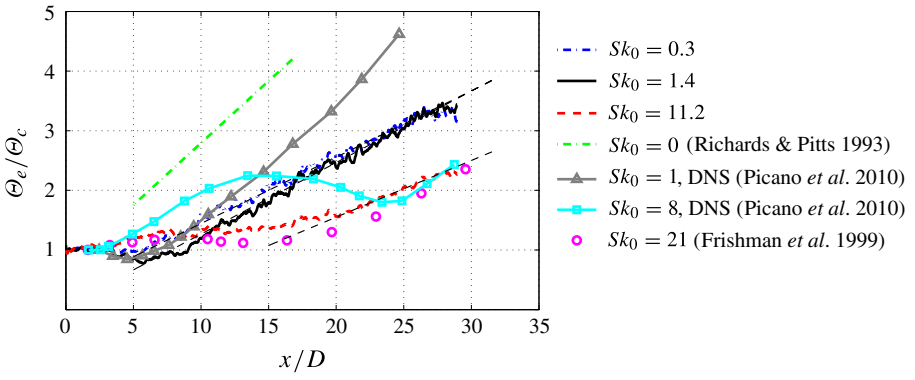

FIGURE 13. (Colour online) The axial evolution of the inverse centreline concentration.

differences between the assumed inflow conditions in the DNS model and the actual inflow conditions of the present experiments. More specifically, the current experimental measurements have shown that the exit concentration profiles are strongly influenced by the Stokes number (see figure 7), while the DNS assumes that the particle concentration at the jet exit is uniform for all exit Stokes numbers. Any jet with a uniform initial particle concentration must inevitably display a hump in the downstream centreline concentration due to the migration of particles from the jet edge to the centreline, as discussed previously. The difference between the current experimental results and the DNS data further highlights the importance of accurately characterising the jet inflow conditions.

Beyond the initial region of strong lateral particle migration, the centreline concentration is observed to decay with x^{-1}, as shown in figure 13. A linear curve fit of this data for $x/D \gtrsim 7$ results in $K_{1,\Theta} = 7.60$, $x_{01,\Theta}/D = -2.51$ and $K_{1,\Theta} = 7.05$, $x_{01,\Theta}/D = -0.47$ for $Sk_0 = 0.3$ and 1.4, respectively. As expected, these decay rates are slightly lower than those measured previously for single-phase jets, namely $4.64 \leqslant K_{1,\Theta} \leqslant 4.81$ (Pitts 1991; Richards & Pitts 1993; Mi *et al.* 2001), as can also be seen from figure 13. The establishment of a linear inverse decay rate much closer to the nozzle than occurs for the $Sk_0 = 11.2$ case is consistent with the much lower local Stokes numbers, consistent with the velocity decay data. Furthermore, a close examination of figure 13 shows that the case $Sk_0 = 1.4$ undergoes a transition from a higher initial decay to a lower one at $x/D \approx 17$ that more closely matches that of the $Sk_0 = 0.3$ case. This, together with the axial evolution of the local Stokes number shown in figure 11, suggests that the transition to a linear decay occurs where the local Stokes number is of order 0.3, although further work is required to confirm this. For the $Sk_0 = 11.2$ case, the measured downstream translation of the 'virtual origin' relative to the low Stokes number cases, which is also observed in the velocity decay, is not only due to the increased local Stokes number, but also to the influence of particle convergence on to the axis through the region of the 'potential core'. A linear curve fit of the inverse centreline concentration data for $x/D \gtrsim 20$ yields $K_{1,\Theta} \approx 8.89$ and $x_{01,\Theta}/D \approx 3.14$.

3.4. *Jet expansion*

Figure 14 presents the velocity half-width as a function of streamwise distance. Consistent with the measurements of the centreline velocity decay (figure 10), the

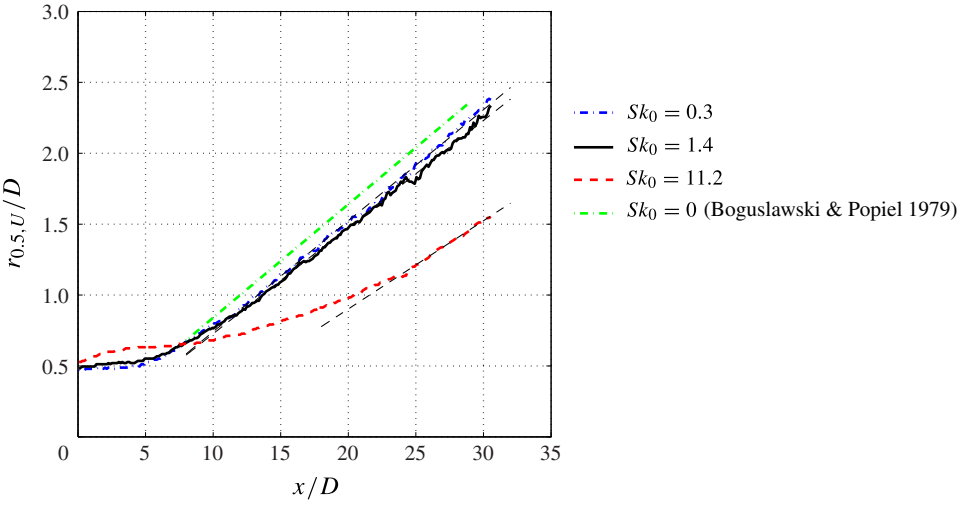

FIGURE 14. (Colour online) The axial evolution of the velocity half-width.

half-widths of the two lower Stokes number cases are very similar, and show a linear growth with streamwise distance for $x/D \gtrsim 10$. In contrast, the $Sk_0 = 11.2$ case does not exhibit a linear decay until $x/D \approx 25$, where the local Stokes number is expected to approach order unity. This result is also consistent with the centreline velocity (figure 10) and concentration (figures 12 and 13) data. This suggests that for the high Sk_0 case, the transition of the local Stokes number from a high-number regime at the jet exit to order unity at far-downstream locations ($x/D \approx 25$) significantly increases the streamwise distance required for the inverse decay and half-widths, of both the velocity and concentration, to exhibit a linear relationship with axial distance. Linear curve fits of the data results in velocity expansion coefficients $K_{2,U} = 0.078$, $K_{2,U} = 0.075$ and $K_{2,U} \approx 0.062$, as well as virtual origins $x_{02,U}/d_\epsilon = 0.45$, $x_{02,U}/d_\epsilon = 0.29$ and $x_{02,U}/d_\epsilon \approx 4.65$ for $Sk_0 = 0.3$, $Sk_0 = 1.4$ and $Sk_0 = 11.2$, respectively. The value of the expansion coefficients found here for the two lower Stokes number cases are in good agreement with previous work, being only slightly lower than the values of $K_{2,U} = 0.08$ (Boguslawski & Popiel 1979) and $K_{2,U} = 0.086$ (Xu & Antonia 2002) found in similar single-phase jets. Similarly, the value found here for the high Stokes number case is only slightly lower than the value of $K_{2,U} = 0.07$ previously measured (Modarress *et al.* 1984*a*) for the dispersed phase at $Sk_0 \approx 13.5$. The lower jet expansion of the current two-phase jet when compared to single-phase jets is consistent with observations of other two-phase jets (Modarress *et al.* 1984*a*; Shuen *et al.* 1985; Hardalupas *et al.* 1989; Sheen *et al.* 1994; Fan *et al.* 1997), and with the lower centreline velocity decay measured in this study (see § 3.3).

The streamwise evolution of the concentration half-width is presented in figure 15. For the $Sk_0 = 1.4$ case, there is a distinct region over the range $4 \lesssim x/D \lesssim 7$ where the jet narrows. This region corresponds to the region where the particles near to the edge of the jet migrate towards the jet centreline (figure 9), thereby reducing the effective concentration half-width of the jet. A similar region is also seen in the $Sk_0 = 0.3$ case over the range $4 \lesssim x/D \lesssim 6$, although this region is not as distinct as the $Sk_0 = 1.4$ case, consistent with the centreline concentration measurements discussed in § 3.3. Linear curve fits of the two low Stokes number cases data yield $K_{2,\Theta} = 0.064$, $x_{02,\Theta} = -3.50$ and $K_{2,\Theta} = 0.075$, $x_{02,\Theta} = 0.97$ for $Sk_0 = 0.3$ and $Sk_0 = 1.4$, respectively. While it has

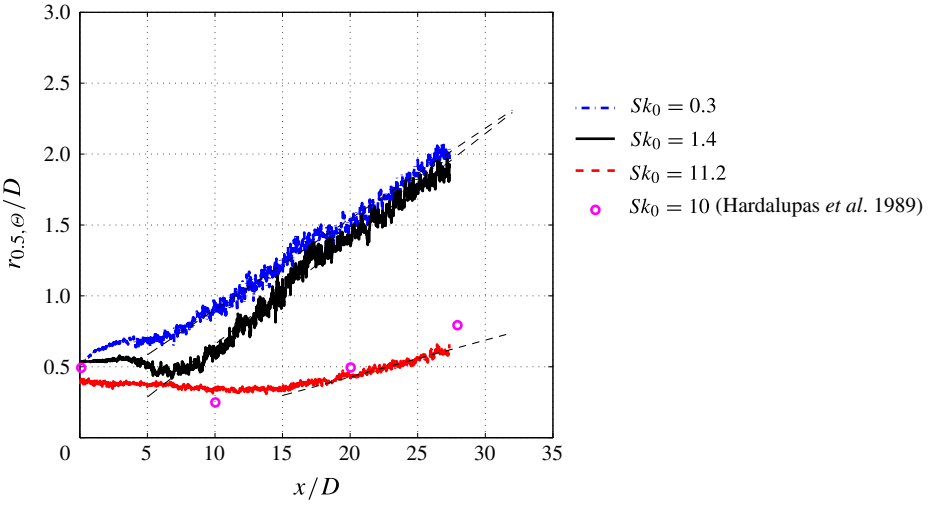

FIGURE 15. (Colour online) The axial evolution of the concentration half-width.

been shown that the rate of expansion of the velocity field in the current study is only slightly lower than that for similar single-phase jets, this is not the case with the concentration field. The expansion of the concentration field is significantly lower than for similar single-phase jets, which have typical concentration expansion coefficients of $0.102 \leqslant K_{2,\Theta} \leqslant 0.108$ (Richards & Pitts 1993; Mi *et al.* 2001). This is further evidence that the concentration field is more sensitive to jet-exit Stokes number than the velocity field. The streamwise evolution of the concentration half-width for the $Sk_0 = 11.2$ case agrees more broadly with experimental measurements by Hardalupas *et al.* (1989) (also shown in figure 15), which were performed for a particle-laden jet at $Sk_0 = 10$. For this case, the jet expansion increases linearly with axial distance for $x/D \gtrsim 20$, with a resultant expansion coefficient of $K_{2,\Theta} \approx 0.026$ and a virtual origin of $x_{02,\Theta} \approx 3.02$.

The jet expansion coefficients, decay coefficients and virtual origins for particle velocity and concentration measured in the current study are shown in tables 5 and 6, along with selected results from measurements of similar single- and two-phase turbulent jets. In summary, the current measurements show that the axial evolution of velocity and concentration decay, as well as jet expansion, of the two-phase jet is lower than for similar single-phase jets, consistent with current knowledge of particle-laden jets (Balachandar & Eaton 2010). This difference between the current two-phase jet and single-phase jets increases with the Stokes number, and is more prominent in the concentration distribution when compared to the velocity distribution.

4. Conclusions

Simultaneous planar measurements of particle velocity and concentration in a series of well-characterised particle-laden, turbulent jets issuing from a long round pipe into a co-flow have revealed that the exit Stokes number has a significant impact on the exit distribution of particle concentration and that this influence also impacts the subsequent evolution of the two-phase jet. The accuracy of these measurements is confirmed by good agreement with existing data and consistency with established knowledge of particle-laden jets. Like earlier work, it is found that the rates of jet

Study	ϕ	Sk_0	Re_D	$K_{1,U}$	$x_{01,U}/d_\epsilon$	$K_{2,U}$	$x_{02,U}/d_\epsilon$
		0.3	10 000	7.43	−2.69	0.078	0.45
Current	0.4	1.4	10 000	6.95	−1.37	0.075	0.29
		11.2	20 000	≈10.03	≈2.63	≈0.062	≈4.65
Modarress *et al.* (1984*a*)	0.32	13.5	13 300	10.5*	−1.46*	—	—
Hussein *et al.* (1994)	—	0	95 500	5.8	4.0	0.094	—
Boguslawski & Popiel (1979)	—	0	>51 000	5.9	−0.5	0.08	—
Xu & Antonia (2002)	—	0	86 000	6.5	2.6	0.086	—

TABLE 5. A comparison of the current velocity measurements with published results of other single- and two-phase turbulent jets. Single-phase experiments are denoted by $Sk_0 = 0$, while an * denotes values that were extracted from published data. It should be noted that measurements of coefficients and virtual origins for the $Sk_0 = 11.2$ case are an estimate, as these values have not converged to a steady value within the measurement region.

Study	ϕ	Sk_0	Re_D	$K_{1,\Theta}$	$x_{01,\Theta}/d_\epsilon$	$K_{2,\Theta}$	$x_{02,\Theta}/d_\epsilon$
		0.3	10 000	7.60	−2.51	0.064	−3.50
Current	0.4	1.4	10 000	7.05	−0.47	0.074	0.97
		11.2	20 000	≈8.89	≈3.14	≈0.026	≈3.02
Mi *et al.* (2001)	—	0	16 000	4.64	4.73	0.102	1.30
Pitts (1991)	—	0	12 000	4.9	0.84	—	—
Richards & Pitts (1993)	—	0	25 000	4.81	−3.44	0.108	6.97

TABLE 6. A comparison of the current concentration measurements with published results of other single- and two-phase turbulent jets. See the caption of table 5 for more information.

spread and decay increase with a decrease in the exit Stokes number, while the length of the 'potential core' is decreased. However, new details about the role of the Stokes number have been revealed by the combination of narrow size distribution of particles, the detailed resolution of the near field and the investigation of the three regimes of jet-exit Stokes number from less than unity, order unity and order 10. Specifically, the current work has shown that:

(*a*) The scalar distribution of the particles at the exit plane of the pipe is strongly dependent on the exit Stokes number. Particles with $Sk_0 \lesssim 1$ are preferentially concentrated towards the jet edge, while particles with $Sk_0 \gg 1$ are preferentially distributed on the axis. It is postulated that these results can be explained by the relative significance of two forces, namely the Saffman lift and turbophoretic force, together with the memory of effects originating from the establishment of the fully developed two-phase flow. Saffman lift, which induces lateral particle migration towards the pipe axis for particles lagging the surrounding fluid, is deduced to dominate for $Sk_0 \gg 1$, while turbophoresis, which induces particle migration towards the pipe wall very close to the pipe boundary (where the particle turbulent kinetic energy is low), is deduced to dominate for $Sk_0 \lesssim 1$. Within the upstream region of the pipe in which the fully developed velocity profiles are established, continuity leads to the particle concentration profile tending towards being inversely proportional to the velocity profile. These findings are consistent with the current data and with the available literature.

Exit Stokes number, Sk_0	Mean particle diameter, $\overline{d}_p$ (μm)	Jet bulk velocity, U_b (m s^{-1})	Exit Reynolds number, Re_D
0.3	10	9	5 000
1.4	10	36	22 500
11.2	40	18	10 000

TABLE 7. A summary of the experimental parameters for the longer pipe length case ($L/D \approx 301.3$). In this case, $D = 9.525$ mm.

(*b*) The above influence of Sk_0 on the exit scalar distributions is significant in the near field and the transition region to a fully developed mean flow field. In particular, for the two lower Stokes number cases, the migration of the particles from the jet edge towards the jet axis causes a near-field hump in the centreline concentration, which subsequently causes a downstream translation of the virtual origin of the centreline decay, and to a lesser extent, of the half-widths.

(*c*) The decrease in the local Stokes number with axial distance through the jet causes the near field of the $Sk_0 = 11.2$ jet to undergo a transition from a high to a low Stokes number regime through the first 25 diameters or so. This effect greatly extends the distance required for the velocity and scalar fields to reach the regime where the inverse decay rate and half-widths, of both the concentration and velocity, increase linearly with axial distance.

Acknowledgements

The authors gratefully acknowledge the financial support of the Australian Government through the Australian Research Council and the Australian Renewable Energy Agency (ARENA). The authors would also like to thank Mr M. R. Chowdhury and Mr I. Saridakis for their useful contributions in the laboratory, as well as the anonymous reviewers for their insightful observations and constructive feedback.

Appendix. Comparison of exit concentration at different pipe lengths

The results reported in the paper were based on experiments utilising a pipe with a length-to-diameter ratio of $L/D \approx 163.8$ and diameter $D = 12.7$ mm. For single-phase flows, this pipe length is sufficiently long to result in a fully developed pipe flow at the exit (Rajaratnam 1976). However, the required pipe length to generate a fully developed two-phase flow at the pipe exit is currently unknown. To assess the effect of pipe length on the exit conditions, the experiments were repeated with a longer pipe of smaller diameter ($D = 9.525$ mm), leading to a length-to-diameter ratio of $L/D \approx 301.3$. The flow conditions of this experiment are shown in table 7.

A comparison of the exit concentrations for both pipe lengths and all three Stokes numbers is shown in figure 16. The concentration profile was chosen instead of the velocity profile for comparison because the velocity field was found to be less sensitive to the L/D ratio than the concentration (scalar) field. The results show that the exit concentration profiles from the two pipes of different L/D ratios are sufficiently close to each other to justify the conclusion that both have converged closely to the asymptotic state. However, the differences in the concentration profiles are also non-zero. It is possible that these differences are, at least in part, attributable to the slight differences in operating conditions, such as the $\overline{d}_p/D$ ratios and Reynolds

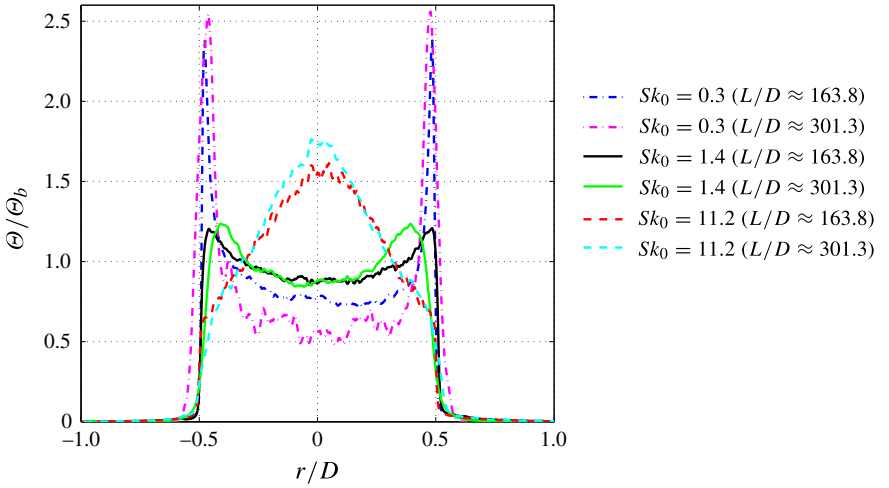

FIGURE 16. (Colour online) A comparison of the exit concentration for two different pipe lengths at all investigated Stokes numbers.

numbers, between the two cases. However, it is also possible that pipe lengths of $L/D > 163.8$ are required to generate a fully developed two-phase flow at the pipe exit. Further work is required to fully resolve this issue.

REFERENCES

ANTONIA, R. A. & BILGER, R. W. 1973 An experimental investigation of an axisymmetric jet in a co-flowing air stream. *J. Fluid Mech.* **61**, 805–822.

ASMOLOV, E. S. 1999 The inertial lift of a spherical particle in a plane Poiseuille flow at large channel Reynolds numbers. *J. Fluid Mech.* **381**, 63–87.

BALACHANDAR, S. & EATON, J. K. 2010 Turbulent dispersed multiphase flow. *Annu. Rev. Fluid Mech.* **42**, 111–133.

BI, W., SUGII, Y., OKAMOTO, K. & MADARAME, H. 2003 Time-resolved proper orthogonal decomposition of the near-field flow of a round jet measured by dynamic particle image velocimetry. *Meas. Sci. Technol.* **14**, L1–L5.

BIRZER, C. H., KALT, P. A. M. & NATHAN, G. J. 2011 The influences of jet precession on large-scale instantaneous turbulent particle clusters. *Intl J. Multiphase Flow* **37**, 394–402.

BIRZER, C. H., KALT, P. A. M. & NATHAN, G. J. 2012 The influences of particle mass loading on mean and instantaneous particle distributions in precessing jet flows. *Intl J. Multiphase Flow* **41**, 12–22.

BOGUSLAWSKI, L. & POPIEL, CZ. O. 1979 Flow structure of the free round turbulent jet in the initial region. *J. Fluid Mech.* **90**, 531–539.

EGGELS, J. G., UNGER, F., WEISS, M. H., WESTERWEEL, J., ADRIAN, R. J., FRIEDRICH, R. & NIEUWSTADT, F. T. 1994 Fully developed turbulent pipe flow: a comparison between direct numerical simulation and experiment. *J. Fluid Mech.* **268**, 175–209.

ELGHOBASHI, S. 2006 An updated classification map of particle-laden turbulent flows. In *Proceedings of the IUTAM Symposium on Computational Multiphase Flow* (ed. S. Balachandar & A. Prosperetti), Springer.

FAIRWEATHER, M. & HURN, J.-P. 2008 Validation of an anisotropic model of turbulent flows containing dispersed solid particles applied to gas–solid jets. *Comput. Chem. Engng* **32**, 590–599.

FAN, J., ZHANG, X., CHEN, L. & CHEN, K. 1997 New stochastic particle dispersion modeling of a turbulent particle-laden round jet. *Chem. Engng J.* **66**, 207–215.

FLECKHAUS, D., HISHIDA, K. & MAEDA, M. 1987 Effect of laden solid particles on the turbulent flow structure of a round free jet. *Exp. Fluids* **5**, 323–333.

FRISHMAN, F., HUSSAINOV, M., KARTUSHINSKY, A. & RUDI, U. 1999 Distribution characteristics of the mass concentration of coarse solid particles in a two-phase turbulent jet. *J. Aero. Sci.* **30**, 51–69.

GILLANDT, I., FRITSCHING, U. & BAUCKHAGE, K. 2001 Measurement of phase interaction in dispersed gas/particle two-phase flow. *Intl J. Multiphase Flow* **27**, 1313–1332.

HARDALUPAS, Y., TAYLOR, A. M. K. P. & WHITELAW, J. H. 1989 Velocity and particle-flux characteristics of turbulent particle-laden jets. *Proc. R. Soc. Lond.* A **426**, 31–78.

HUSSEIN, H. J., CAPP, S. P. & GEORGE, W. K. 1994 Velocity measurements in a high Reynolds-number, momentum-conserving, axisymmetric, turbulent jet. *J. Fluid Mech.* **258**, 31–75.

KALT, P. A. M., BIRZER, C. H. & NATHAN, G. J. 2007 Corrections to facilitate planar imaging of particle concentration in particle-laden flows using Mie scattering, Part 1: Collimated laser sheets. *Appl. Opt.* **46**, 5823–5834.

KALT, P. A. M. & NATHAN, G. J. 2007 Corrections to facilitate planar imaging of particle concentration in particle-laden flows using Mie scattering, Part 2: Diverging laser sheets. *Appl. Opt.* **46**, 7227–7236.

KIM, J., MOIN, P. & MOSER, R. 1987 Turbulence statistics in fully developed channel flow at low Reynolds number. *J. Fluid Mech.* **177**, 133–166.

KUSSIN, J. & SOMMERFELD, M. 2002 Experimental studies on particle behaviour and turbulence modification in horizontal channel flow with different wall roughness. *Exp. Fluids* **33**, 143–159.

LAATS, M. K. & FRISHMAN, F. A. 1970 Assumptions used in calculating the two-phase jet. *Izv. Akad. Nauk SSSR Mekh. Zhidk. Gaza* **5**, 186–191 (in Russian).

LIEPMANN, D. & GHARIB, M. 1992 The role of streamwise vorticity in the near-field entrainment of round jets. *J. Fluid Mech.* **245**, 643–668.

MCLAUGHLIN, J. B. 1991 Inertial migration of a small sphere in linear shear flows. *J. Fluid Mech.* **224**, 261–274.

MCLAUGHLIN, J. B. 1993 The lift on a small sphere in wall-bounded linear shear flows. *J. Fluid Mech.* **246**, 249–265.

MI, J., NOBES, D. S. & NATHAN, G. J. 2001 Influence of jet exit conditions on the passive scalar field of an axisymmetric free jet. *J. Fluid Mech.* **432**, 91–125.

MODARRESS, D., TAN, H. & ELGHOBASHI, S. 1984*a* Two-component LDA measurement in a two-phase turbulent jet. *AIAA J.* **22**, 624–630.

MODARRESS, D., WUERER, J. & ELGHOBASHI, S. 1984*b* An experimental study of a turbulent round two-phase jet. *Chem. Engng Commun.* **28**, 341–354.

MOSTAFA, A. A., MONGIA, H. C., MCDONELL, V. G. & SAMUELSEN, G. S. 1989 Evolution of particle-laden jet flows: a theoretical and experimental study. *AIAA J.* **27**, 167–183.

MULLINGER, P. & JENKINS, B. 2008 *Industrial and Process Furnaces: Principles, Design and Operation*. Elsevier.

NATHAN, G. J., KALT, P. A. M., ALWAHABI, Z. T., DALLY, B. B., MEDWELL, P. R. & CHAN, Q. N. 2012 Recent advances in the measurement of strongly radiating, turbulent reacting flows. *Prog. Energy Combust. Sci.* **38**, 41–61.

NATHAN, G. J., MI, J., ALWAHABI, Z. T., NEWBOLD, G. J. R. & NOBES, D. S. 2006 Impacts of a jet's exit flow pattern on mixing and combustion performance. *Prog. Energy Combust. Sci.* **32**, 496–538.

PICANO, F., SARDINA, G., GUALTIERI, P. & CASCIOLA, C. M. 2010 Anomalous memory effects on the transport of inertial particles in turbulent jets. *Phys. Fluids* **22** (5), 051705.

PITTS, W. M. 1991 Reynolds number effects on the mixing behaviour of axisymmetric turbulent jets. *Exp. Fluids* **11**, 135–141.

PREVOST, F., BOREE, J., NUGLISCH, H. J. & CHARNAY, G. 1996 Measurements of fluid/particle correlated motion in the far field of an axisymmetric jet. *Intl J. Multiphase Flow* **22**, 685–701.

RAFFEL, M., WILLERT, C. W. & KOMPENHANS, J. 1998 *Particle Image Velocimetry: A Practical Guide*. Springer.

RAJARATNAM, N. 1976 *Turbulent Jets*. Elsevier.

REEKS, M. W. 1983 The transport of discrete particles in inhomogeneous turbulence. *J. Aero. Sci.* **14**, 729–739.

RICHARDS, C. D. & PITTS, W. M. 1993 Global density effects on the self-preservation behaviour of turbulent free jets. *J. Fluid Mech.* **254**, 417–435.

SAFFMAN, P. G. 1965 The lift on a small sphere in a slow shear flow. *J. Fluid Mech.* **22**, 385–400.

SHEEN, H. J., JOU, B. H. & LEE, Y. T. 1994 Effect of particle size on a two-phase turbulent jet. *Exp. Therm. Fluid Sci.* **8**, 315–327.

SHUEN, J. S., SOLOMON, A. S. P. & ZHANG, Q. F. 1985 Structure of particle-laden jets: measurements and predictions. *AIAA J.* **23**, 396–404.

SMOOT, L. D. & SMITH, P. J. 1985 *Coal Combustion and Gasification*. Plenum Press.

THRING, M. W. & NEWBY, M. P. 1953 Combustion length of enclosed turbulent jet flames. In *Fourth International Symposium on Combustion*, Williams & Wilkins.

TSUJI, Y., MORIKAWA, Y., TANAKA, T., KARIMINE, K. & NISHIDA, S. 1988 Measurement of an axisymmetric jet laden with coarse particles. *Intl J. Multiphase Flow* **14**, 565–574.

XU, G. & ANTONIA, R. A. 2002 Effect of different initial conditions on a turbulent round free jet. *Exp. Fluids* **33**, 677–683.

YAMAGUCHI, H. 2008 *Engineering Fluid Mechanics*. Springer.

YOUNG, J. & LEEMING, A. 1997 A theory of particle deposition in turbulent pipe flow. *J. Fluid Mech.* **340**, 129–159.